Extracting relevant physiological information from polar auxin transport data in Panax ginseng

Boot, C.J.M.; Hille, S.C.; Korthout, H.A.A.J.; Libbenga, K.R.; Duijn, A. van

Journal of Plant Physiology 262 (2021) 153436

Contents lists available at ScienceDirect

Journal of Plant Physiology

journal homepage: www.elsevier.com/locate/jplph

Extracting relevant physiological information from polar auxin transport data in *Panax ginseng*

Kees J.M. Boot [a,b], Sander C. Hille [a,c], Henrie A.A.J. Korthout [b], Kees R. Libbenga [a], Bert van Duijn [a,b,*]

[a] *Plant Biodynamics Laboratory, Institute of Biology, Leiden University, 2333 BE, Leiden, the Netherlands*
[b] *Fytagoras, 2333 BE, Leiden, the Netherlands*
[c] *Mathematical Institute, Leiden University, 2333 CA, Leiden, the Netherlands*

ARTICLE INFO

Keywords:
Auxin
indole-3-acetic acid
Polar transport
Mathematical model
Panax ginseng

ABSTRACT

Background: Measuring polar auxin transport (PAT) in plants and drawing conclusions from the observed transport data is only meaningful if these data are being analysed with a mathematical model which describes PAT. In this report we studied the polar auxin transport in *Panax ginseng* stems of different age and grown on different substrates.
Methods: We measured polar IAA transport in stems using a radio labelled IAA and analysed the transport data with a mathematical model we developed for *Arabidopsis*.
Results: We found that PAT in ginseng stems, as compared to *Arabidopsis* inflorescence stems, has a 2-fold lower transport velocity and a 3-fold lower steady state auxin flux.
Conclusion: We were able to pinpoint two physiological parameters that influenced the observed transport characteristics in ginseng which differ from *Arabidopsis*, namely an increase in immobilization together with a reduced reflux of IAA from the surrounding tissue back to the transporting cells.

1. Introduction

For more than a century the plant hormone auxin (Indole-3-acetic acid, IAA) has been the subject of a wide variety of research topics ranging from auxin perception, gene regulation, signal transduction and transport (Friml, 2003; Friml and Palme, 2002; Salehin et al., 2015). Especially, the long-distance polar auxin transport (PAT) has intrigued many scientists (Adamowski and Friml, 2015; Friml and Palme, 2002). When radio-labelled auxin became available in the 1960s a myriad of PAT measurements in all kinds of tissues were published (see Kramer et al., 2011). The interpretation of these data, however, proved to be difficult and was not unambiguous. Therefore, it was necessary to first develop a concept and a model for PAT. The first concept that described PAT at the cellular level was postulated by the chemiosmotic theory, which stated that the uptake and efflux of IAA in cells could be augmented by specific auxin carrier proteins and where polarity is being caused by the asymmetrical distribution of the efflux carriers. The driving force for the transport is provided by the proton-motive force (Raven, 1975; Rubery and Sheldrake, 1974). Later a new class of extended models for PAT were published (Goldsmith et al., 1981; Mitchison, 1980). With the advance of Arabidopsis genetics soon genes for putative auxin influx carrier proteins, like the AUX1/LIKE-AUX1 (AUX/LAX) (Peret et al., 2012), and auxin efflux proteins candidates, like the PIN-FORMED (PIN) (Krecek et al., 2009) and P_GLYCOPROTEIN, MULTIDRUG RESISTANCE, and ATP-BINDING CASSETTE SUBFAMILY B (PGP, MDR, and ABCB) (Geisler and Murphy, 2006) were cloned and PAT measurements in pin1 mutant plants showed a strong decrease in auxin transport capacity (Okada et al., 1991). Although there is a consensus among most scientists that the current view on how PAT is regulated at the cellular level is valid, there are still some important points that have to be taken into consideration before such a firm conclusion can be drawn. For instance, the transport data for pin1 were never analyzed with the use of existing models and the models themselves were also never experimentally tested. Furthermore, the methods that were used to measure PAT were not really suited for measuring the dynamics of PAT.

We were confronted with these problems, when we got involved in long-distance auxin transport as part of an extensive research project on

* Corresponding author at: Fytagoras BV, Sylvius Laboratory, Sylviusweg 72, 2333BE, Leiden, the Netherlands.
E-mail address: bert.vanduijn@fytagoras.com (B. van Duijn).

https://doi.org/10.1016/j.jplph.2021.153436
Received 2 April 2021; Received in revised form 10 May 2021; Accepted 13 May 2021
Available online 15 May 2021

the development and architecture of the root system of *Panax ginseng*. Ginseng is an important medical herb that is widely cultivated in North America, Korea, China and Japan (Anoja et al., 1999; Wu and Zhong, 1999). In particular, root architecture plays an important role in the ginseng economic value, the main aspects being the number of lateral roots and the thickness of the main root. The more the root resembles a human form, which is according to Chinese tradition believed to represent the essence of earth crystalized in a human form, the more valuable the root becomes (Baranov, 1966). Since auxin, and in particular PAT, plays an important role in processes such as branching, lateral root formation and secondary root growth (Gallavotti, 2013; Smith and De Smet, 2012; Vanneste and Friml, 2009; Wheeldon and Bennett, 2021), our initial focus was on how to extract relevant information from PAT measurements. In order to tackle the problems as outlined above, we started to study PAT in inflorescence stems of the model plant *Arabidopsis thaliana* because of the availability of a wide range of (putative) PAT mutants and developed a mathematical model that describes the dynamics of PAT at the macroscopic level and which enables us to quantify various parameters that govern PAT fluxes, such as velocity, immobilization and exchange of the hormone with its direct environment in the PAT system (Boot et al., 2016).

Here we report validation of our mathematical model-based analysis of PAT data as part of the ginseng program. We present a full analysis of PAT data from a few growth stages of laboratory cultured ginseng plants. In particular, a change in the exchange parameters that regulate the exchange of auxin with the surrounding tissue of cells involved in PAT, predicts a possible lower abundancy or inhibition of auxin-influx carriers, such as the AUX/LAX1-3 proteins.

2. Results

2.1. Growth conditions

In the literature no data are available on how to grow ginseng plants derived from seeds on a laboratory scale. Therefore, we tried several different substrates to grow plants on, such as soil, stonewool plugs and liquid medium (Supplement 1). We observed that plants grown on soil had lesser accumulation of anthocyanin in their basal stem parts as compared to plants grown on either stonewool plugs or liquid medium. Anthocyanin production is mostly a sign for stress (any unfavourable condition that affects plant metabolism, growth or development in plants) (Tattini and Gould, 2015). Therefore, we decided to use plants which were grown on soil for our initial experiments.

2.2. PAT measurements in ginseng plants

For our initial PAT measurements we used 16 mm-long basal stem segments from 2.5-weeks-old ginseng plants grown on soil. Fig. 1 gives the transport characteristics of a representative PAT experiment (Fig. 1A: average efflux profile of nine individual stem segments, Fig. 1B: average corresponding tissue profile). After a time lag of 125 min the efflux profile showed a transient efflux followed by a steady state flux of ^{3}H-IAA of about 0.65 fmoles/min. The tissue profile showed a relatively strong accumulation at the donor end, followed by an almost equal lower amount of IAA in the two middle parts and again an accumulation at the receiver end. To determine that we were really looking at polar auxin transport we also did a PAT experiment were we reversed the orientation of the stem segments or added an auxin transport inhibitor NPA at 5×10^{-6} M. Both treatments nearly completely inhibited the accumulation of ^{3}H-IAA in the receiver wells and also the tissue profiles showed no accumulation of ^{3}H-IAA in the 8–16 mm parts of the stem segments in contrast to the polar orientation of the stem segments (Fig. 1).

We compared these ginseng transport profiles with PAT measurements from 6.5-weeks-old *Arabidopsis* inflorescence stems which we consider to be a standard method for measuring PAT (Boot et al., 2016).

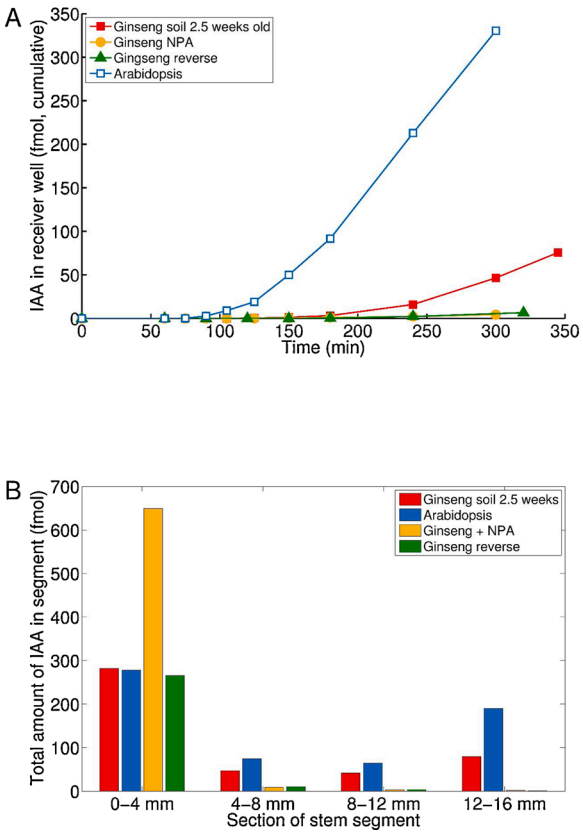

Fig. 1. Efflux profile (A) and tissue profile (B) of PAT measurements with ^{3}H-IAA in ginseng stem segments compared to PAT data from Arabidopsis inflorescence stems.

The efflux profile of *Arabidopsis* stems showed a much shorter lag time of around 75 min, which was 50 min shorter than that of ginseng stems (Fig. 1A). The steady state flux in *Arabidopsis* was 1.96 fmoles/min, nearly three times that of ginseng. The tissue profile of *Arabidopsis* showed an 1.5 times higher accumulation of IAA in the middle parts and a nearly 2.5 times increase at the receiver end as compared to ginseng. Interestingly, the accumulation at the donor ends were nearly the same.

Although some quantitative differences can be observed between ginseng and *Arabidopsis* PAT data, the overall patterns for the transport data are the same. To better understand the observed differences in the PAT transport profiles between ginseng and *Arabidopsis* plants, we analyzed the data with our macroscopic advection-diffusion model developed for PAT measurements in *Arabidopsis* as described in (Boot et al., 2016).

2.3. Analysis of transport data with the advection-diffusion model

Fig. 2A gives a schematic overview of the model we used to analyze the obtained transport data. It consists of an active auxin transport compartment *u*, a *w* compartment which surrounds the u compartment and an immobilization compartment *z* which is situated in the *u* compartment. The interactions between these compartments are given by the equations shown in Fig. 2B

Table 1 gives the parameter values which were used to simulate the transport data from the pooled 9 individual stem segments from both ginseng and *Arabidopsis*. Fig. 3A, C, E and B, D, F show the quality of the simulation of both the transport profiles and the tissue profiles for ginseng (2.5 weeks and 2 months old) and *Arabidopsis* (6.5 weeks old).

The parameter V represents the macroscopic transport velocity, and as can be seen from Table 1, the V for ginseng was about half that for *Arabidopsis*. The values for V for *Arabidopsis* and ginseng, as predicted by

A

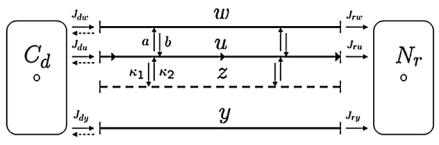

B

$$\partial_t u = D_u \Delta u - V \partial_x u - au + bw - \kappa_1 u + \kappa_2 z$$
$$\partial_t w = D_w \Delta w + au - bw$$
$$\partial_t y = D_y \Delta y$$
$$\partial_t z = \kappa_1 u - \kappa_2 z$$
$$V_d \frac{dC_d}{dt} = J_{du} + J_{dw} + J_{dy}$$
$$\frac{dN_r}{dt} = J_{ru} + J_{rw} + J_{ry}$$
$$J_{du} = P^+_{du} S_u \cdot C_d - P^-_{du} \cdot u(0) \quad \text{etc.}$$
$$J_{ru} = P^-_{ru} \cdot u(L)$$

Fig. 2. Schematic representation of the model (A) with the associated equations (B).

Table 1
Parameter values for the simulation of PAT data sets from ginseng and Arabidopsis stems. In bold the major observed differences between the parameter sets are given.

Age		Ginseng 2,5 weeks	*Arabidopsis* 6,5 weeks		Ginseng 2 months
Diffusion	Du	2×10^{-10}	2×10^{-10}	m2/s	2×10^{-10}
	Dw	7×10^{-11}	7×10^{-11}	m2/s	7×10^{-11}
	Dy	2×10^{-11}	2×10^{-11}	m2/s	2×10^{-11}
Velocity	V	**1.95×10^{-6}**	**3.65×10^{-6}**	m/s	**1.93×10^{-6}**
Exchange	a	2×10^{-4}	2×10^{-4}	1/s	2×10^{-4}
	b	7×10^{-4}	7×10^{-4}	1/s	**2.2×10^{-4}**
Uptake at donor	P^+du	1.25×10^{-6}	1.9×10^{-6}	m/s	1.25×10^{-6}
	P^-du	1.5×10^{-8}	1.5×10^{-8}	m/s	1.5×10^{-8}
	P^+dw	1.35×10^{-6}	2.2×10^{-6}	m/s	2×10^{-6}
	P^-dw	1.5×10^{-8}	1.5×10^{-8}	m/s	1.5×10^{-8}
	P^+dy	1.36×10^{-7}	0.92×10^{-7}	m/s	1.38×10^{-7}
	P^-dy	1.5×10^{-8}	1.5×10^{-8}	m/s	1.5×10^{-8}
Immobilization	*κ1*	2.2×10^{-5}	1.35×10^{-5}	1/s	**4×10^{-5}**
	κ2	1×10^{-6}	1×10^{-6}	1/s	1×10^{-6}
Efflux at receiver	Pr	3.6×10^{-8}	2.2×10^{-8}	m/s	0.84×10^{-8}
Anatomy	S	1.05×10^{-6}	1.44×10^{-6}	m2	1.6×10^{-6}
	SVB/S	0.099	0.134		0.104
	alpha	0.32	0.32	%	0.32
IAA donor concentration	Cd	1.14×10^{-4}	1.11×10^{-4}	M	1.54×10^{-4}
Free versus bound IAA	u + w	Data 80 Sim 80	Data 87 Sim 87	%	Data 79 Sim 79
	z	Data 20 Sim 20	Data 13 Sim 13	%	Data 21 Sim 21
Value cost function		7.3 %	4.3 %		8.7 %

our model, are 1.3 cm/h and 0.7 cm/h, respectively. The parameters *a* and *b* are phenomenological parameters that describe the exchange rates between the transporting cells and the surrounding tissues, where *a* represents the flux out of the transport cells and *b* the reflux from the surrounding tissues back to the auxin transporting cells. No difference in these parameters were observed between ginseng and *Arabidopsis*. The parameters kappa 1 and 2 (*κ1* and *κ2*) are in our model involved in the immobilization of IAA in the transporting cells. Parameter *κ1* is involved in the increase of immobilized IAA, while parameter *κ2* is involved in the release of immobilized IAA. A slight increase in *κ1* was seen for ginseng as compared to *Arabidopsis*. Next we measured the immobilization of IAA in ginseng and *Arabidopsis* stems by extracting ^{3}H-IAA from the stems after performing a PAT experiment. Thin-Layer Chromatography (TLC) analysis showed that *Arabidopsis* stems had approximately 87 % of their ^{3}H-IAA in the unbound free form and only 13 % of the ^{3}H-IAA was found to be in the unfree bound state, most likely through conjugation (Woodward and Bartel, 2005). For the ginseng stems a slight increase in the bound form of IAA was observed as compared to *Arabidopsis*, respectively from 20 % to 13 %. These amounts of free and bound IAA were also included as data points for the mathematical analysis with our model.

2.4. PAT measurements in older ginseng plants

Since roots of ginseng plants grown on soil developed strongly over time in our experimental setup, we measured PAT in 2-months-old ginseng stems to see if the change in root morphology correlates with altered PAT and corresponding parameter values. Older ginseng stems showed about the same lag time but had a strongly reduced steady state flux of ^{3}H-IAA of around 0.33 fmol/min (Fig. 4A). The tissue profile (Fig. 4B), however, shows a strong, nearly 3.5-fold increase of ^{3}H-IAA accumulation in all 4 stem segments as compared to 2.5-weeks old ginseng stems.

The parameter values of the simulation of the transport data for the 2-months-old ginseng stems with our model are shown in Table 1 and the simulation of the transport data are shown in Fig. 3E and F. The V for young and old ginseng plants was approximately the same, but we had to decrease parameter *b* 3.5-fold as compared to younger ginseng stems. Parameter *κ1* shows a 2-fold increase in 2-months-old ginseng stems as compared to 2.5-weeks-old ginseng plants. The measured lower steady state flux together with the increase in the tissue profile that we observed in the 2-months-old ginseng stems could be caused by a combination of a decrease in parameter *b*, which results in a reduced reflux of IAA from the *w*-compartment which surrounds the transporting cells (*u*-compartment) and accordingly to a higher IAA amount in the surrounding tissues (*w*-compartment) together with an increase of parameter *κ1* resulting in more immobilization of IAA in the transporting cells (*z*-compartment) resulting in the observed transport data. Our model shows that this is indeed the case. For young ginseng stems the model predicts that 78 % of IAA is in the *u*-compartment with 22 % in the *w*-compartment, while for the 2-months-old ginseng stems the model shows a clear shift between the two compartments, with only 44 % of IAA in the *u*-compartment while 56 % of IAA resides in the *w*-compartment. Also, according to the model, the amount of IAA in the z-compartment increases from 24 % in young stems to 32 % in the older stems. So the changes in the two parameters b and *κ1* can fully explain the observed transport characteristics between young and old ginseng stems.

2.5. Growth of ginseng on different substrates

We also grew ginseng plants on stonewool plugs, and analyzed the PAT of 3-weeks and 4-months-old ginseng plants. No significant difference in efflux profiles were observed for these plants grown on plugs as compared to plants grown on soil (Fig. 4C). Again the older plants have a longer lag time and show a decreased auxin transport capacity as compared to younger plants. The tissue profiles of 4-months-old plants grown on both substrates shows an increase in amounts of ^{3}H-IAA accumulation when compared to young plants and the profiles look more gradient-like without an accumulation at the receiver ends (Fig. 4D).

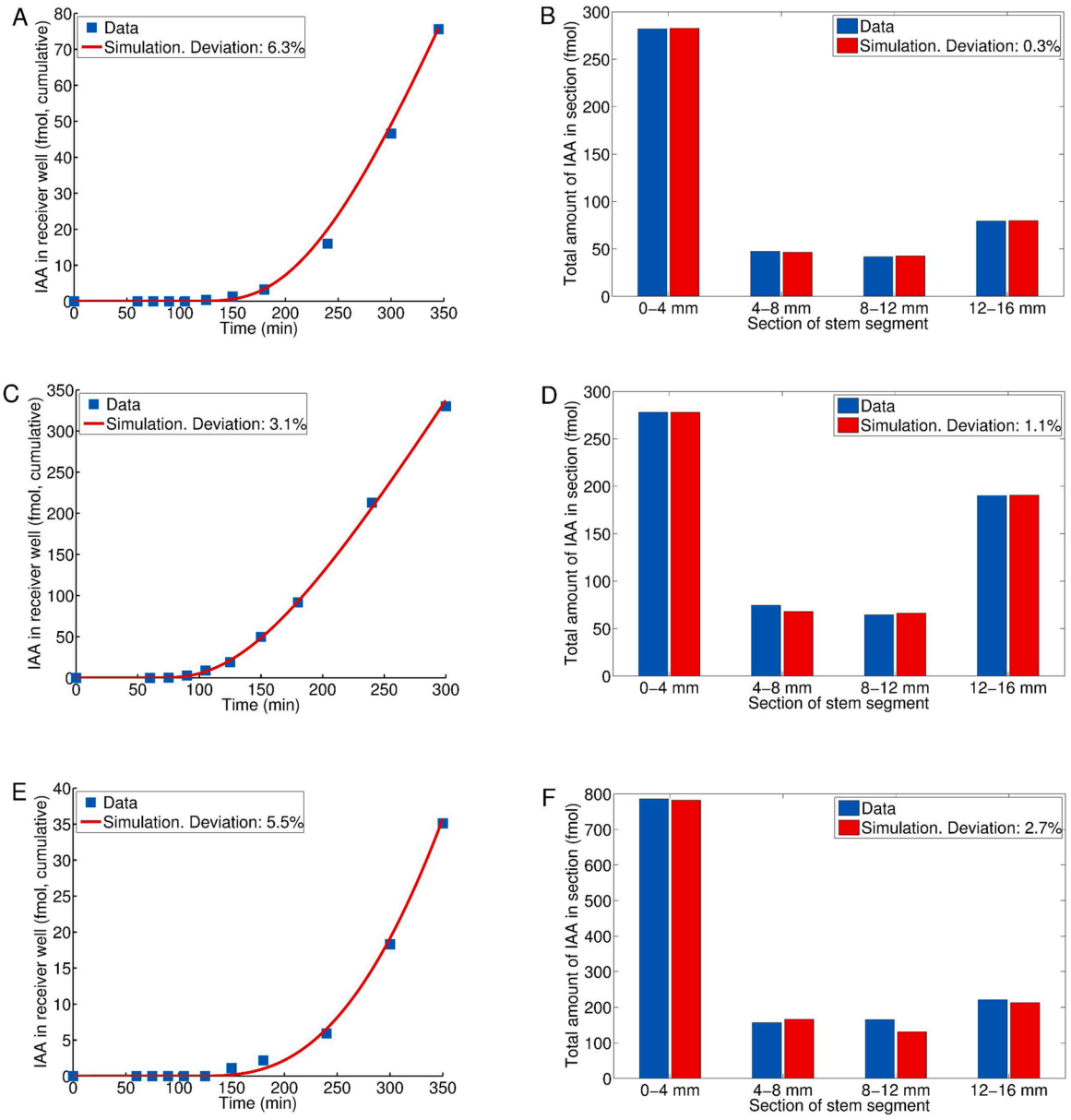

Fig. 3. Simulation of the transport data and the tissue profile data with the parameters from Table 1. 3A,B: Ginseng 2.5 weeks; 3C,D: Arabidopsis 6.5 weeks; 3E,F: Ginseng 2 months.

2.6. Root morphology and ginsenosides content of young versus old ginseng plants

Looking at the roots of young and old plants we observed a different morphology between both young and old roots and also between roots that were either grown on soil or plugs (Supplement 2). Roots of older ginseng plants grown on soil showed secondary root growth and the roots became shorter as compared to young ginseng roots. Roots that were grown on plugs showed an increased thickening as compared to soil grown roots, were shorter and also had shorter lateral roots.

We were interested to see if this difference in root morphology was also reflected in their ginsenosides content (Fig. 5). Both young and old ginseng roots grown on plugs or soil had roughly the same amount of Rg1 and Re, the two major ginsenosides that can be found in ginseng roots.

3. Discussion

In our previous article we showed that our advection-diffusion model extended with immobilization and exchange between transporting cells and surrounding tissues could describe PAT dynamics in *Arabidopsis* inflorescence stems at the macroscopic level in a very reliable manner (Boot et al., 2016). With this model we can accurately estimate transport velocities and steady-state fluxes. Here we analyzed, for the first time, the transport dynamics of PAT in ginseng stems of different ages and compared them to standard PAT in *Arabidopsis* inflorescence stems.

We observed a clear difference in the velocity V as predicted by our model between *Arabidopsis* and ginseng of nearly a factor two: 1.3 cm/hr and 0.7 cm/hr, respectively. These velocities are well within the range of 0.12–1.8 cm/h of observed transport velocities found for different plant tissues as reviewed in (Goldsmith et al., 1981). Furthermore (Mitchison, 1980), concluded based on a cellular model made for PAT that the auxin transport velocity should be in the range of 0.5 to maximal 2.0 cm/hr. Kramer found by compiling data from 119 speed values from 35

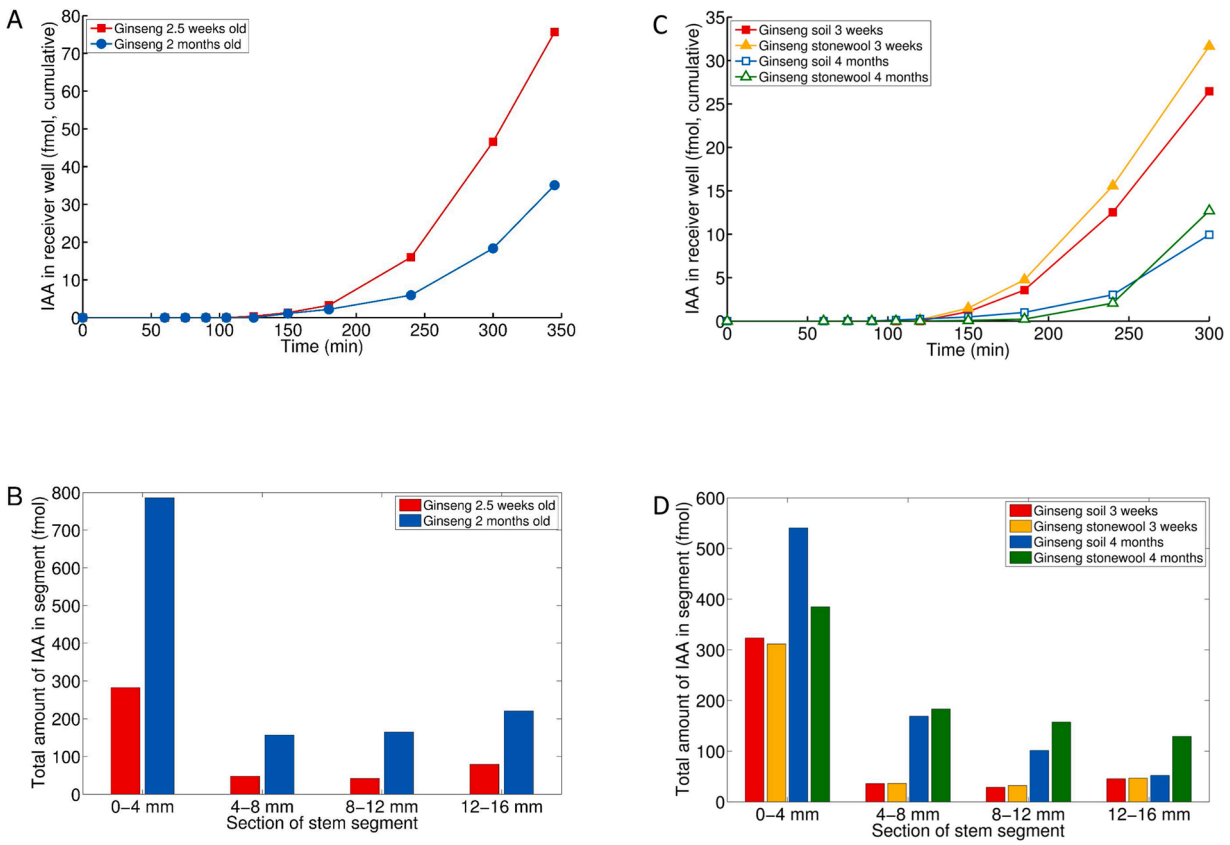

Fig. 4. Efflux profile (A) and tissue profile (B) of 2-months-old ginseng stems. For comparison the data of 2.5-weeks-old ginseng stem segments from Fig. 2 were also included. Efflux profiles (C) and tissue profiles (D) of ginseng plants grown on soil or stonewool plugs for 3 weeks and 4 months.

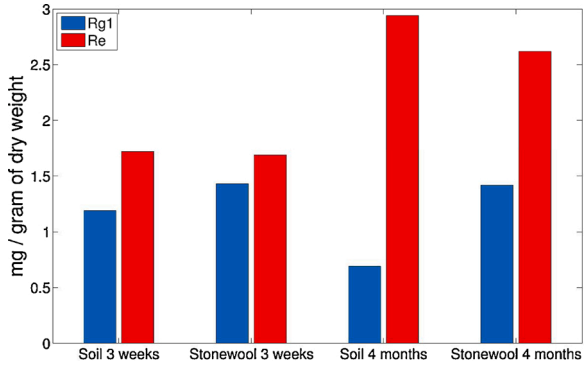

Fig. 5. Ginsenosides content of young (3-weeks-old) and old (4-month-old) roots from ginseng plants grown either on soil or stonewool plugs.

different plant species a median speed of 0.63 cm/hr (Kramer et al., 2011). The V for ginseng stems we observed in our experiments is very close to this value, while the V we found for *Arabidopsis* is relatively high as compared to this median value. Therefore, we conclude that the V in ginseng stems falls in the category of normal transport velocities, while the V in *Arabidopsis* inflorescence stems falls into the group of plant tissues with the highest auxin transport velocity, as was also found for coleoptiles which had an average speed of 1.2 cm/hr (Kramer et al., 2011).

Another aspect of PAT in ginseng stems is the steady state flux. Again here we see a clear difference between ginseng and *Arabidopsis*, in which *Arabidopsis* inflorescence stems have a 3-fold higher steady state flux of auxin as compared to ginseng stems. The steady state flux is determined by several different factors. First of all the immobilization rate of auxin in the transporting tissue, if this rate is high, less auxin will be available for transport. In ginseng stems we see a slight increase in the immobilization parameter $\kappa 1$ of about 2- to 3-fold as compared to *Arabidopsis*. This higher increase in immobilization is reflected in the relative amount of bound versus free which we measured in ginseng stems using TLC. The bound fraction slightly increases to 20 % of the total IAA amount in these stems as to only 13 % in *Arabidopsis* stems. This is further supported by the prediction of our model that in young ginseng stems more IAA is being localized in the z-compartment as compared to *Arabidopsis* stems, 24 % to 19 %, respectively. In older ginseng stems this percentage increases even more to 32 %. Based on our TLC analysis we can only distinguish between bound and free forms of IAA. The nature of the bound IAA fraction is unclear. From the literature it is well-known that plants can conjugate free IAA to sugars or amino acids, leading to permanently or temporarily storage of IAA. Furthermore, IAA can also be broken down by specific IAA-oxidases. It is for us impossible at this moment to differentiate between these different mechanisms. It is possible that in older ginseng stems the amount of IAA conjugation could be increased perhaps as a result of an increased leakage of IAA to the w-compartment. Secondly, leakage from the transporting tissue to the surrounding cells plays an important role in determining steady state fluxes, the higher the leakage the lower the flux will be. In our previous publication (Boot et al., 2016) we showed that the IAA influx carriers play an important role in maintaining IAA in the transporting cells by redirecting IAA that has leaked out of the transporting cells back into the transport stream. A quadruple mutant which lacked all four AUX1/LAX1-3 influx carriers from *Arabidopsis* (Bainbridge et al., 2008; Peret et al., 2012) was still able to transport IAA, but with a strongly reduced auxin transport capacity. We could simulate the obtained transport data from this quadruple mutant with our model by strongly decreasing the parameter *b* by approximately 35-fold (Boot et al., 2016). In the 2-months old ginseng stems we also observed a decrease in the

IAA transport capacity and this could be simulated by reducing parameter *b* about 3.5 times as compared to 2.5-weeks-old ginseng stems. Our model predicts a clear shift between the IAA amounts in the *u*- and *w*-compartments from young and older ginseng stems, with 78 % in the *u*-compartment for young stems and only 44 % in the *u*-compartment for old stems (Fig. 6). This predicts that in these older stems either the amount of AUX1/LAX1-3 proteins or their activity could be reduced. Interestingly, a comparison between *Arabidopsis* and young ginseng stems with our model, each having the same parameter *b* values, showed that in both stems 78 % of the IAA was in the u-compartment (Fig. 6).

Another important factor that influences the steady state flux is the number of transporting cells in the transporting tissue. Since wild type *Arabidopsis* inflorescence stems have on average 8–9 vascular bundles per stem, while ginseng stems only have three, a part of the difference in auxin flux can be accounted for by the lower number of transporting cells between these two plant species. One other aspect is the velocity and the time at which the steady state flux is calculated. Since *Arabidopsis* has a higher transport velocity the steady state flux will be reached earlier than in ginseng with a nearly 2-fold lower transport velocity. The steady state flux for ginseng as obtained from the efflux transport data can therefore be an underestimation of the actual flux. With the use of our model we can predict the steady state fluxes at longer time points by simulating efflux profiles after for instance 10 h instead of the usual 5 h which we used in our experiments. By doing this for *Arabidopsis* we obtained a steady state flux after 10 h of 2.3 fmol/min. Comparing this to the value we found after 5 h, which was 1.96 fmol/min, we see that for *Arabidopsis* the initial observed steady state flux was nearly optimal. If we look at the steady state flux at 5 and 10 h for the 2.5-weeks-old ginseng stems we again see that the flux was already nearly maximal, 0.65 fmol/min against 0.7 fmol/min, respectively. For the 2-months-old ginseng stems we see that we strongly underestimated the flux after 5 h of transport, namely 0.33 fmol/min against 0.82 fmol/min after 10 h of presumed incubation with ^{3}H-IAA. But even after 10 h the transport capacity of auxin in ginseng stems remains approximately 3-times lower as compared to that in *Arabidopsis* inflorescence stems.

The extracted relevant physiological information thus obtained from the transport data by using our model again stresses the point that the observed differences in V, efflux profiles, tissue profiles and steady state fluxes can only be interpreted with the use of a model. By just looking at the raw transport data it is impossible to draw any conclusions from these data and to really understand what could be the cause for the observed differences in measured transport characteristics and changes in underlying physiological alterations.

Our data show that changes in PAT characteristics, for instance in young versus old ginseng stems, correlates with changes in root morphology. How this correlation is translated in real cause and effect is not clear yet. Auxin is involved in various aspects of root morphology, such as primary root growth, lateral root formation, vascular differentiation, root hair elongation and gravitropism. These developmental responses are a result of tightly regulated auxin maxima and minima established through auxin biosynthesis and auxin transport in the root. Current models infer an important role for PIN proteins and members of the AUX/LAX family of proteins for establishing these centres of auxin maxima and minima. However, these current models are mainly based on the expression patterns of the transport proteins while there is no direct evidence for auxin flow at the cellular level. By measuring PAT and analyzing the transport characteristics with our model we hope that this could lead ultimately to a more fundamental platform for a better understanding of the role of PAT in root morphology and as such to practical applications in ginseng production.

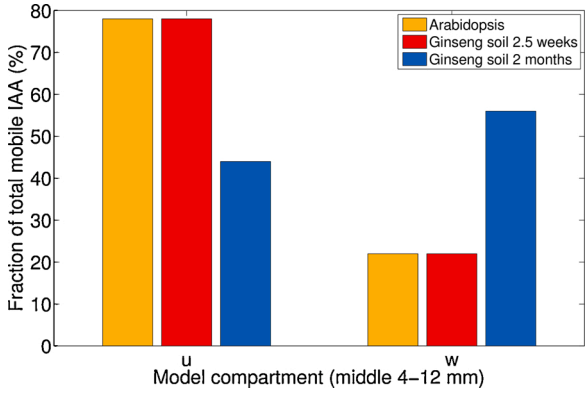

Fig. 6. Distribution of auxin between the u- and w-compartment as predicted by our model in the 4-12 mm part of stem segments from 6,5 weeks-old Arabidopsis, 2,5 weeks-old and 2 months-old ginseng stems.

4. Material and methods

4.1. Plant material and growth conditions

Panax ginseng seeds that underwent a double cold stratification (seeds that underwent a cold stratification were subjected to a second cold stratification after being placed at 21 °C for a certain period) were kept a month at 4 °C on wetted filter paper. Germinated ginseng seeds and Arabidopsis thaliana ecotype Col-0 plants were grown on a mixture of 9:1 substrate soil and sand (Holland Potgrond) at either 18 °C or 21 °C, respectively, with a 16 -hrs photoperiod, and 70 % relative humidity. Ginseng seeds were also cultured on stonewool plugs (Grodan, The Netherlands) at the same culture conditions.

4.2. Polar auxin transport measurements

PAT experiments were performed as described in (Boot et al., 2016). In short, 9 individual 16-mm-long segments were cut from the most basal part of the main stems of plants and placed between one common donor well and 9 individual receiver wells. The donor and receiver wells were filled with MA medium supplemented with 10 mM MES (pH = 4.8). To the donor wells ^{3}H-labelled IAA (3-[5(n)- ^{3}H] IAA, specific activity 25 Ci/mmol (925 GBq/mmol), Scopus Research BV, Veenendaal, The Netherlands) to a final concentration of 10^{-4} mol/m^{3} (10^{-7} M) was added. At regular time intervals receiver wells were emptied and replaced by fresh medium. Radioactivity of the samples was measured in an LKB liquid scintillation counter. For determining tissue profiles, segments were cut into 4-mm-long pieces and transferred to scintillation liquid and counted.

4.3. Microscopy

For light microscopy, segments from the basal part of inflorescences of *Arabidopsis* or ginseng stems were cut from the plant and kept in 4 % paraformaldehyde. Transverse sections were made with a table-bench microtome at a thickness of 150 μm and mounted on a glass slide in water. The sections were then photographed with a Zeiss Axioplan Imaging upright light microscope (Carl Zeiss, Oberkochen, Germany), equipped with a Zeiss Axiocam MRC 5 digital camera. Sections were used to determine the anatomical parameters S (the cross-sectional area of a stem segment) and S_{vb} (sum of cross-sectional areas of vascular bundles). By cutting and weighing images of the sections the percentage of S_{vb} per stem segment was determined.

4.4. Thin-Layer chromatography (TLC) analysis

Ginseng stem segments and *Arabidopsis* inflorescence stems were ground in liquid N_2 and extracted two times with ethanol. Samples were spotted on silica gel60 F254 fluorescent aluminium TLC plates (Merck, Darmstadt, Germany) and separated in a solvent containing n-hexane: ethylacetate:isopropanol:acetic acid (40:20:5:1, v/v) (Chung et al.,

2003). After running, the TLC plate was divided into nine 1.5 cm sections, which were cut off and added to liquid-scintillation vials and counted in a LKB liquid scintillation counter.

4.5. Ginsenosides measurements

Ginsenosides extraction from the roots was performed by pressurized solvent extraction (PSE) using a Speed Extractor E-916 (BÜCHI Labortechnik AG, Flawil, Switzerland). Root samples were dried and homogenized to fine powder and were mixed with 9 ml fat free quartz sand (0.3−0.9 mm, BÜCHI Labortechnik AG, Flawil, Switzerland). The mixture was extracted with 70 % ethanol (J.T. Baker, USA) and 30 % H_2O (Honeywell Riedel de Haen, the Netherlands) in 10 ml stainless steel extraction cells at 100 ºC and 100 bar. Two cycles (heat-up time of 1 min, hold time of 1 min for cycle 1 and 2 min for cycle 2, and discharge time of 2 min) were performed. After extraction the samples were dried and resolved in 70 % Methanol (Sigma Aldrich, USA) and analyzed by HPLC (Agilent Technologies 1200 series, USA) using a C18 column (Kinetex-EVO, Phenomenex, the Netherlands) and a H_2O / Acetonitrile (LiChrosolv Merck, Ger) gradient.

4.6. Mathematical modelling, numerical simulation and data fitting

The model we used is described in (Boot et al., 2016). Numerical simulation of the mathematical model was performed in the COMSOL Multiphysics package (version 4.2.0.150), using the generalized-alpha time-dependent solver, which was coupled to MATLAB (version R2008b) via COMSOL Multiphysics LiveLink for the data fitting procedure. After manual parameter tuning using visual inspection to make sure that all values remained in a physiologically reasonable range, we got a good starting point for further automated fine tuning. The automated fine tuning used alternatingly the method of gradient descent and linear search in opposite gradient direction, to reduce the number of numerical gradient evaluations, which are computationally time consuming. As measures for the quality of fit served: (1) the sum of absolute deviations between data points and simulation in the transport profile relative to the total cumulative amount measured in the receiver well at the end of the experiment, (2) the sum of absolute deviations between data points and simulation in the tissue profile relative to the total measured amount of IAA in the tissue and (3) the absolute deviation in percentage between measured and simulated immobilisation ratio. These three dimensionless quantities were added, yielding a total deviation that is minimised. The optimisation procedure was stopped when the three sub-measures were below 7.5 %, 5 % and 1 %, respectively, and the total deviation below 10 %.

5. Conclusion

We found that polar auxin transport in ginseng stems, as compared to Arabidopsis inflorescence stems, has a 2-fold lower transport velocity and a 3-fold lower steady state auxin flux.

We were able to pinpoint two physiological parameters that influenced the observed transport characteristics in ginseng which differ from Arabidopsis, namely an increase in immobilization together with a reduced reflux of IAA from the surrounding tissue back to the transporting cells.

CRediT authorship contribution statement

Kees J.M. Boot: Conceptualization, Data curation, Formal analysis, Investigation, Methodology, Writing - original draft, Writing - review & editing. **Sander C. Hille:** Conceptualization, Investigation, Methodology, Data curation, Formal analysis. **Henrie A.A.J. Korthout:** Formal analysis, Investigation. **Kees R. Libbenga:** Conceptualization, Data curation, Formal analysis, Investigation, Methodology, Writing - original draft, Writing - review & editing. **Bert van Duijn:** Conceptualization, Data curation, Supervision, Writing - review & editing, Funding acquisition.

Declaration of Competing Interest

The authors Kees J. M. Boot, Sander C. Hille, Henrie A.A.J. Korthout, Kees R. Libbenga and Bert van Duijn declare that there are no conflicts of interest with regard to the research, results and the text of the manuscript entitled “Extracting relevant physiological information from polar auxin transport data in Panax ginseng” that is submitted to The Journal of Plant Physiology.

Appendix A. Supplementary data

Supplementary material related to this article can be found, in the online version, at doi:https://doi.org/10.1016/j.jplph.2021.153436.

References

Adamowski, M., Friml, J., 2015. PIN-dependent auxin transport: action, regulation, and evolution. Plant Cell 27, 20–32.
Anoja, S., Attelle, A.S., Wu, J.A., Yuan, C.S., 1999. Ginseng pharmacology multiple constituents and multiple actions. Biochem. Pharmacol. 58, 1685–1693.
Bainbridge, K., Guyomarc'h, S., Bayer, E., Swarup, R., Bennett, M., Mandel, T., Kuhlemeier, C., 2008. Auxin influx carriers stabilize phyllotactic patterning. Genes Dev. 22, 810–823.
Baranov, A., 1966. Recent advances in our knowledge of the morphology, cultivation and uses of Ginseng (Panax ginseng C. A. Meyer). Econ. Bot. 20, 403–406.
Boot, K.J.M., Hille, S.C., Libbenga, K.R., Peletier, L.A., van Spronsen, P.C., van Duijn, B., Offringa, R., 2016. Modelling the dynamics of polar auxin transport in inflorescence stems of Arabidopsis thaliana. J. Exp. Bot. 67, 649–666.
Chung, K.R., Shilts, T., Ertürk, Ü., Timmer, L.W., Ueng, P.P., 2003. Indole derivatives produced by the fungus Colletotrichum acutatum causing lime anthracnose and postbloom fruit drop of citrus. FEMS Micr. Lett. 226, 23–30.
Friml, J., 2003. Auxin transport – shaping the plant. Curr. Opin. Plant Biol. 6, 7–12.
Friml, J., Palme, K., 2002. Polar auxin transport – old questions and new concepts? Plant Mol. Biol. 49, 273–284.
Gallavotti, A., 2013. The role of auxin in shaping shoot architecture. J. Exp. Bot. 64, 2593–2608.
Geisler, M., Murphy, A.S., 2006. The ABC of auxin transport: the role of p-glycoproteins in plant development. FEBS Lett. 580, 1094–1102.
Goldsmith, M.H.M., Goldsmith, T.H., Martin, M.H., 1981. Mathematical analysis of the chemosmotic polar diffusion of auxin through plant tissues. Proc. Natl. Acad. Sci. U. S.A 78, 976–980.
Kramer, E.M., Rutschow, H.L., Mabie, S.S., 2011. AuxV: a database of auxin transport velocities. Trends Plant Sci. 16, 461–463.
Krecek, P., Skupa, P., Libus, J., Naramoto, S., Tejos, R., Friml, J., Zazimalova, E., 2009. The Pin-formed (PIN) protein family of auxin transporters. Genome Biol. 10, 249.
Mitchison, G.J., 1980. The dynamics of auxin transport. Proc.R.Soc.Lond. B. 209, 489–511.
Okada, K., Ueda, J., Komaki, M.K., Bell, C.J., Shimura, Y., 1991. Requirement of the auxin polar transport system in early stages of Arabidopsis floral bud formation. Plant Cell 3, 677–684.
Peret, B., Swarup, K., Ferguson, A., Seth, M., Yang, Y., Dhondt, S., James, N., Casimiro, I., Perry, P., Syed, A., Yang, H., Reemmer, J., Venison, E., Howells, C., Perez-Amador, M.A., Yun, J., Alonso, J., Beemster, G.T.S., Laplaze, L., Murphy, A., Nennett, M.J., Nielsen, E., Swarup, R., 2012. AUX/LAX genes encode a family of auxin influx transporters that perform distinct functions during Arabidopsis development. Plant Cell 24, 2874–2885.
Raven, J.A., 1975. Transport of Indoleacetic acid in plant cells in relation to pH and electrical potential gradients, and its significance for polar IAA transport. New Phytol. 74, 163–172.
Rubery, P.H., Sheldrake, A.R., 1974. Carrier-mediated auxin transport. Planta 118, 101–121.
Salehin, M., Bagchi, R., Estelle, M., 2015. SCFTIR1/AFB-based auxin perception: mechanism and role in plant growth and development. Plant Cell 27, 9–19.
Smith, S., De Smet, I., 2012. Root system architecture: insights from Arabidopsis and cereal crops. Phil. Trans. R. Soc. B 367, 1441–1452.
Tattini, M., Gould, Kevin S., 2015. Multiple functional roles of anthocyanins in plant-environment interactions. Environ. Exp. Bot. 119, 4–17.
Vanneste, S., Friml, J., 2009. Auxin: a trigger for change in plant development. Cell 136, 1005–1016.
Wheeldon, C.D., Bennett, T., 2021. There and back again: an evolutionary perspective on long-distance coordination of plant growth and development. Semin. Cell Dev. Biol. 109, 55–67.
Woodward, A.W., Bartel, B., 2005. Auxin: regulation, action, and interaction. Ann. Bot. 95, 707–735.
Wu, J., Zhong, J.J., 1999. Production of ginseng and its bioactive components in plant cell culture: current technological and applied aspects. J. Biotechnol. 68, 89–99.